

Tunable Photocarrier Dynamics in CuS Nanoflakes under Pressure Modulation

Xiuxiu Han, Xiaoli Ma, Qing Miao, Xiaoxian Zhang,* Dawei He,* Xiaohui Yu,* and Yongsheng Wang

Cite This: *ACS Omega* 2024, 9, 22248–22255

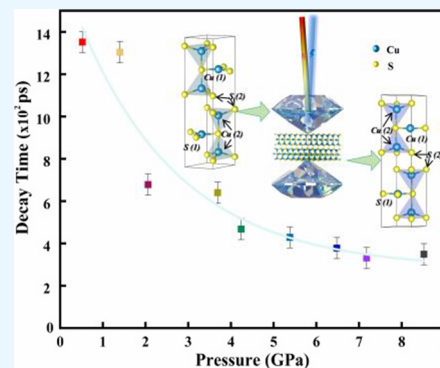
Read Online

ACCESS |

Metrics & More

Article Recommendations

ABSTRACT: Two-dimensional materials with a unique layered structure have attracted intense attention all around the world due to their extraordinary physical properties. Most importantly, the internal Coulomb coupling can be regulated, and thus electronic transition can be realized by manipulating the interlayer interaction effectively through adding external fields. At present, the properties of two-dimensional materials can be tuned through a variety of methods, such as adding pressure, strain, and electromagnetic fields. For optoelectronic applications, the lifetime of the photogenerated carriers is one of the most crucial parameters for the materials. Here, we demonstrate effective modulation of the optical band gap structure and photocarrier dynamics in CuS nanoflakes by applying hydrostatic pressure via a diamond anvil cell. The peak differential reflection signal shows a linear blueshift with the pressure, suggesting effective tuning of interlayer interaction inside CuS by pressure engineering. The results of transient absorption show that the photocarrier lifetime decreases significantly with pressure, suggesting that the dissociation process of the photogenerated carriers accelerates. It could be contributed to the phase transition or the decrease of the phonon vibration frequency caused by the pressure. Further, Raman spectra reveal the change of Cu–S and S–S bonds after adding pressure, indicating the possible occurrence of structural phase transition. Interestingly, all of the variation modes are reversible after releasing pressure. This work has provided an excellent sight to show the regulation of pressure on the photoelectric properties of CuS, exploring CuS to wider applications that can lead toward the realization of future excitonic and photoelectric devices modulated by high pressure.



INTRODUCTION

Two-dimensional (2D) materials beyond graphene and their van der Waals heterostructure have created tremendous interest.^{1–4} Due to their thickness-tunable exceptional electrical, chemical, thermal, and optical properties, 2D layered materials have made significant progress in field-effect transistors,⁵ photovoltaic devices,⁶ photodetectors,⁷ optical modulators,⁸ and integrated circuits.⁹ The optical properties of 2D materials are closely related to their photocarriers, which are generated from free electron–hole pairs or excitons.¹⁰ The dynamical properties of photocarriers, such as carrier thermalization, hot carrier dynamics, exciton formation, transport, and recombination, are critical factors to the performances of optoelectronic and phase-change electronic devices. Hence, understanding the photocarrier dynamics of target materials is essential. Recently, more studies have focused on time-resolved optical techniques of photocarrier dynamics in 2D materials, including ultrafast laser spectroscopy,^{11–13} transient THz spectroscopy,^{14–16} and time-resolved photoluminescence,^{17–20} and have been successful to reveal insight on various aspects of photocarriers.

Due to the unique layered structure, 2D materials can not only show the thickness-tunable properties but more

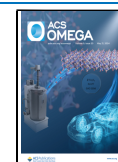
importantly, the electronic transition can be realized by regulating the interlayer interaction through effective external manipulation,²¹ such as temperature, pressure, strain, and electromagnetic.^{22–30} Among these methods, pressure presents a unique ability of effectively modulate the interlayer interaction in 2D layered materials, change the electronic structures,³¹ and even promote phase transition.^{32–34} Recently, Guo et al.³⁵ has proved that pressure processing can effectively reduce the exciton binding energy of 2D perovskite $\text{Cs}_2\text{PbI}_2\text{Cl}_2$ from 133 to 78 meV. Xia et al. demonstrated that the interlayer coupling of 2H-stacked $\text{WSe}_2\text{–MoSe}_2$ heterostructures can be adjusted by using pressure engineering. Band changeover can be generated by pressure, resulting in a clear evolution and transition of interlayer excitons.³⁶ The band structure for the $\text{WS}_2/\text{MoSe}_2$ heterostructure can also be tuned by high

Received: February 9, 2024

Revised: April 17, 2024

Accepted: April 30, 2024

Published: May 13, 2024



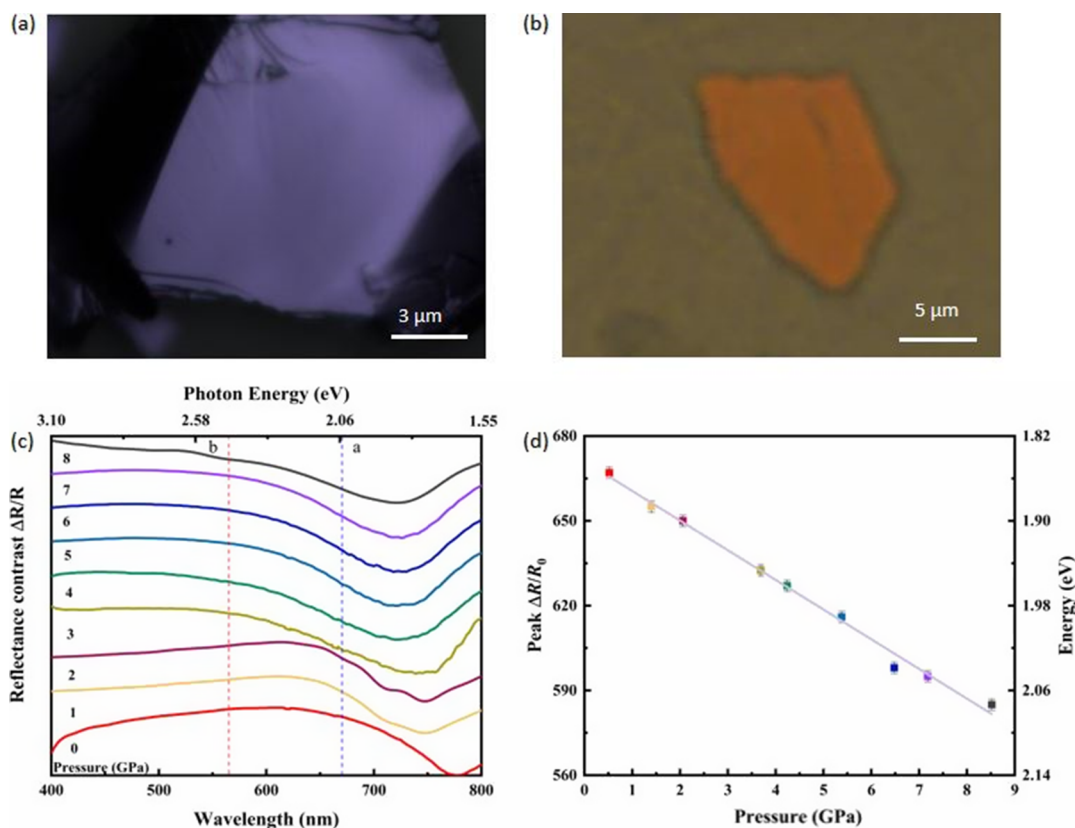


Figure 1. (a) Microscope image of the mechanically exfoliated CuS nanoflakes at standard atmospheric pressure and (b) under the pressure of ~ 8 GPa. (c) Reflectance contrast spectra of the CuS nanoflakes under different pressures. (d) The peak signal of the peak differential reflection signal of the CuS nanoflakes as a function of the probe wavelength under different pressure conditions and is fitted.

pressure, which enhanced the interlayer exciton behavior and revealed the robust peak of interlayer excitons.³⁷ The essence of optoelectronic phenomena under pressure proceeding is due to its high-pressure modulation of microscopic optoelectronic processes at material interfaces.^{38,39}

However, there are rarely reports on the tunable dynamics by phase transition under high pressure, which may be due to the absence of an in situ spectroscopy system with pressure and the difficulty in the fabrication of high-quality samples inside the high-pressure chamber. Here, an in situ spectroscopy system is set up that can achieve the measurements of microscopic transient absorption, PL, and Raman under high pressure. The tunable optical band gap and the photocarrier dynamics are investigated in copper monosulfide (CuS) nanoflakes regulated by pressure. CuS is mostly used as the hole-transporting material for solar cells;^{40,41} at the same time, as a layered transition metal chalcogenide, it also has the advantage of strong nonlinear optical response^{42–44} which can be applied to photodetectors⁴⁵ and other fields. We observed that under high pressure, the optical band gap moves monotonously and the photocarrier lifetime decreases significantly, resulting in the acceleration of carrier dissociation speed by nearly 10 times. The results of steady-state absorption and Raman spectrum indicated that the changes of optical band gap and carrier lifetime are attributed to the phase transition and the phonon vibration frequency. This work opens up an effective method for studying the properties of pressure-tunable optoelectronic materials.

RESULTS AND DISCUSSION

Figure 1a shows a typical optical image of relatively large-scale and uniform CuS microflakes (size: $30 \times 20 \mu\text{m}$; thickness: $10 \mu\text{m}$). The optical microscope image of the CuS nanoflakes in the DAC under the same reflection conditions at about 8 GPa is shown in Figure 1b. We can observe that the color of CuS changes from blue to orange-brown under pressure. This intuitive change in color makes us suspect that the absorption of the material was changed due to the pressure. To further confirm this speculation, the reflectance contrast spectra of the material under pressure are studied, as shown in Figure 1c. In the limit of weak reflective contrast (such for transparent substrates), the reflective contrast is proportional to the sample's absorption,⁴⁶ and this approximation is very beneficial for understanding the absorption of materials under high pressure. Here, the reflection contrast is defined as $\Delta R/R_0 = (R_S - R_Q)/R_Q$. R_S and R_Q are the reflectance of the sample and the substrate, respectively. We found that the absorption peak of CuS nanoflakes has a straightforward blueshift process with pressure (from the dashed line a to b) and became weaker and weaker, which is consistent with the previous report.⁴⁷

To investigate pressure regulation on the optical band gap, we perform probe wavelength measurements of the transient absorption spectrum in a CuS nanoflake. In the previous work, a weak peak centered at $\sim 636 \text{ nm}$ with about 200 nm width could be observed on the photoluminescence (PL) spectrum of the CuS nanoflake.⁴⁸ Combined with its PL spectrum, we did a differential reflection spectroscopic experiment over an extensive spectral range. A 410 nm pump pulse with a fluence of about $27.8 \mu\text{J}/\text{cm}^2$ is used in this experiment. The peak

Table 1. Parameter Setting and Data Analysis of Transient Absorption Spectrum

pressure (GPa)	0.52	1.40	2.06	3.69	4.24	5.38	6.48	7.18	8.52
peak (nm)	667	655	650	632	627	616	598	595	585
ODB (eV)	1.86	1.89	1.90	1.96	1.98	2.01	2.07	2.08	2.12
lifetime ($\times 10^3$ ps)	1.35	1.30	0.68	0.64	0.47	0.42	0.38	0.33	0.35

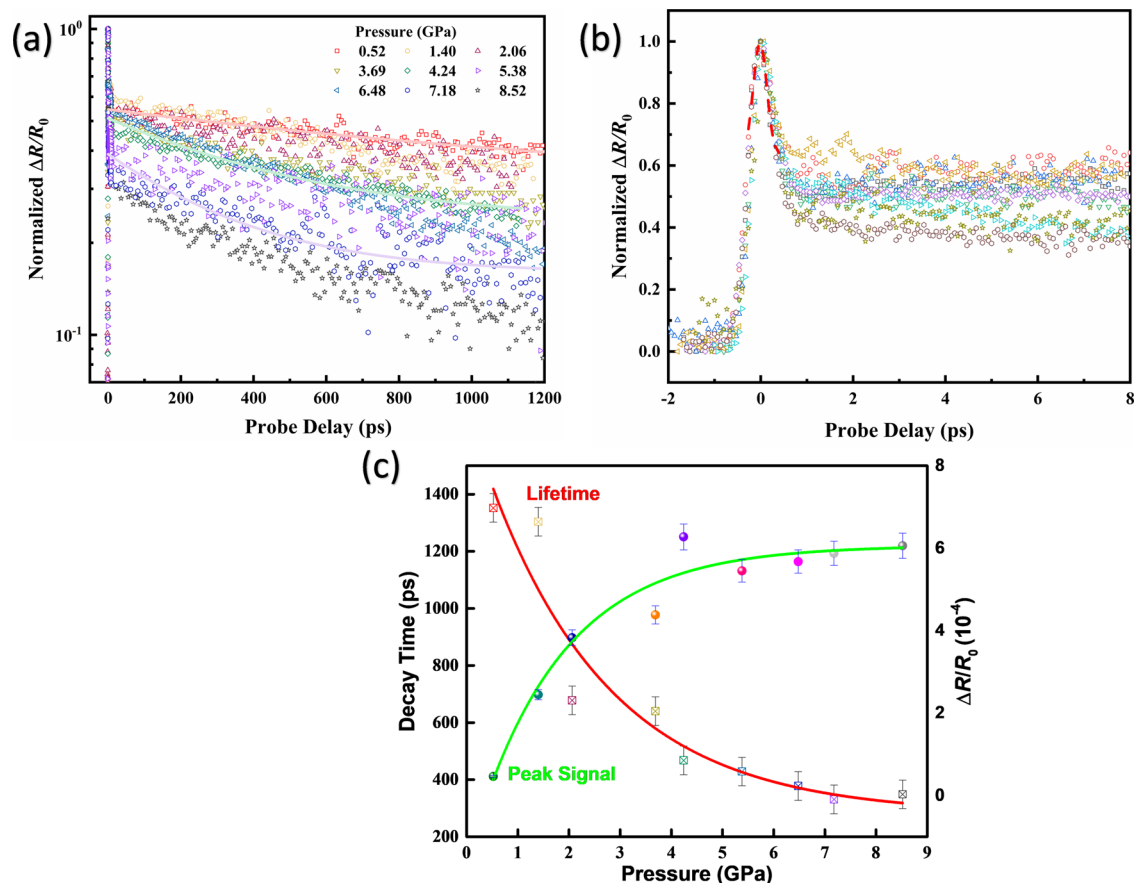


Figure 2. (a) Differential reflection signal as a function of the probe delay under different pressure conditions. The solid curves are fits. (b) Same as (a) but over a short time range near zero delay. The dashed curves represent a Gaussian function with a fwhm of 0.35 ps and its integral. (c) Red line represents single-exponential fits to the lifetime of the photocarrier as a function of the pressure. The green line is the fit to the peak signal of the photocarrier as a function of the pressure. All error bars reflect the uncertainties in the fit.

differential reflection signal is measured as a function of probe wavelength by selecting the probe delay that corresponds to the signal's maximum value. This ensures that the most accurate and representative data are obtained for further analysis. Then, we extract the highest peak signals under different pressures and optimum probe wavelength in Figure 1d left and right axes, respectively. Given that the differential reflection signal peaks occur precisely when the probe resonates with the direct optical band gap,¹⁰ this finding unequivocally establishes the existence of a direct optical band gap in CuS under varying pressures. The direct optical band gap in Figure 1d (right axis) shows a pronounced tendency with the pressure increase, and we can figure out a distinct blueshift up to about 0.3 eV (see Table 1 for specific values). When decompressed, we found it is reversible. Such a regular and exciting phenomenon should be studied. The blueshift behavior of the direct optical band gap could be due to the following two factors: (i) the lattice distortion caused by pressure, such as the bond length between Cu–S and S–S, leads to the change of the electronic structure; (ii) the phase structure changes due to the lattice distortion.

Subsequently, we study the photocarrier dynamics of CuS nanoflakes under different pressure conditions by measuring the differential reflection signal. The colored hollow icons with different shapes in Figure 2a show the results measured with different pressure conditions. We normalize the data, as shown by the curves in Figure 2a. In order to show the lifetime changes caused by pressurization more clearly, we only choose three fitting curves under 0.52, 4.24, and 7.18 GPa to present. The dynamics have a fast component of less than 1 ps, and a slow one persists for more than 300 ps. The slow process can be attributed to the recombination of photocarriers, i.e., photocarrier lifetime,⁴⁹ and the pulse width limits the fast process. Upon investigation, we discovered that the 667 nm probe (1.85 eV) is specifically tuned to align with the band gap of CuS. Meanwhile, the 410 nm pump (3.02 eV) injects photocarriers, manifesting as free electron–hole pairs, with an energy surplus exceeding several hundred millielectronvolts. However, the peak signal was observed at a very early probe delay, suggesting that the hot carriers alter the band-edge absorption instantaneously. Figure 2b shows the signal near the zero probe delay of Figure 2a. To quantify the feature, we fit

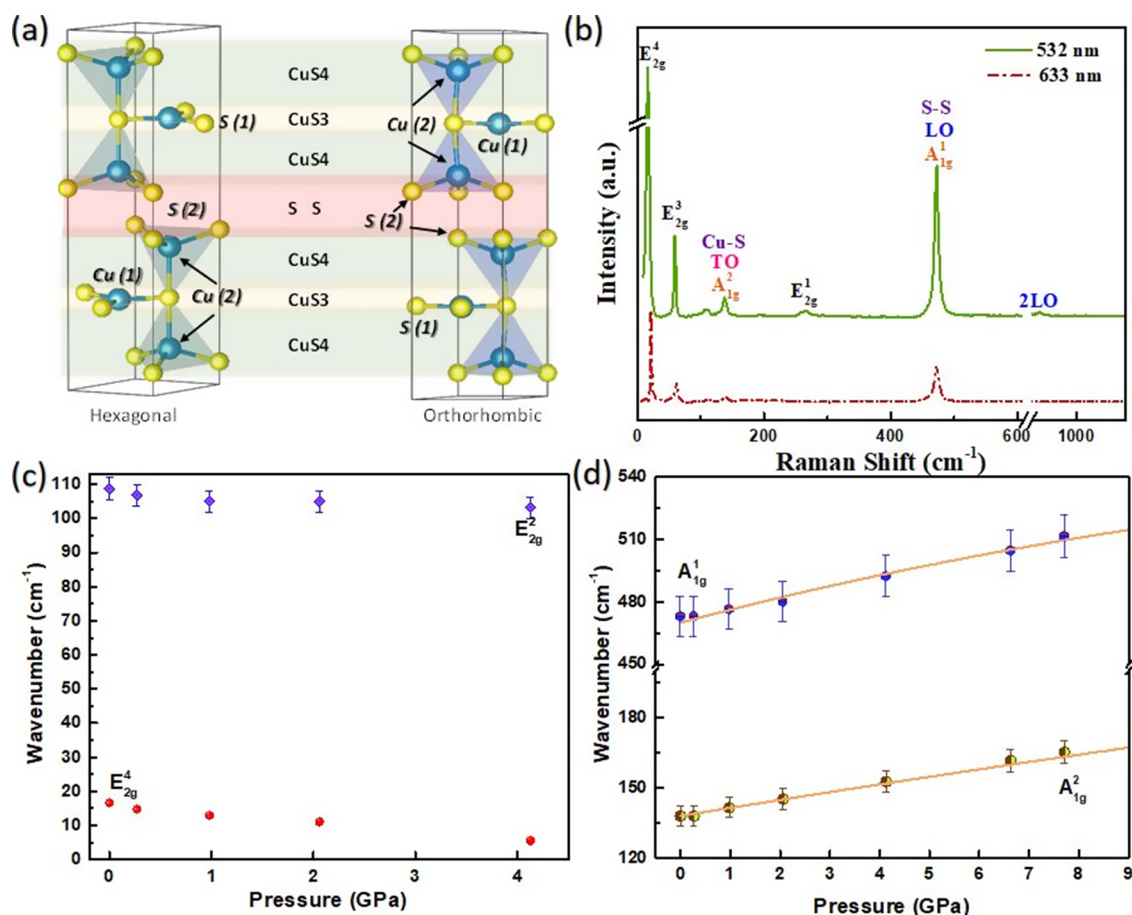


Figure 3. (a) Hexagonal (left) and orthorhombic (right) crystal structure of CuS. (b) Raman spectra of bulk CuS; the green line is excited by a continuous-wave 532 nm and the red dashed line is by 633 nm. (c) Phonon frequencies of bulk CuS as a function of pressure with E_{2g}^4 mode at ~ 108 cm^{-1} . (d) Same as (c) but for the A_{1g} mode.

the peak near zero delay with a Gaussian function, as shown by the red dashed line in Figure 2b. At each pressure condition, the peak signal on an ultrafast time scale can perfectly coincide, and all time constants are independent of the pump fluence. The fwhm of 350 fs is close to the used pulse widths. Drawing upon the obtained results, we can confidently attribute this peak to the direct nonlinear interaction occurring between the pump and probe pulses. This interaction could encompass processes such as sum-frequency generation or two-photon absorption, both of which are unrelated to the photocarriers.

The slow decay of the signal can be satisfactorily fit by an exponential function $\Delta R/R_0 = A \exp(-t/\tau_1) + B$. The time constants obtained from these fits are summarized in the table. The time constant at 0.52 GPa is in the same order as the previous reports at ambient conditions.⁵⁰ Moreover, the periodic oscillation in the signal is due to the excitation of coherent optical photons.⁵¹ The photocarrier lifetime decreases with increasing pressure; all of the photocarrier lifetime constants are plotted in Figure 2c, and the red line has been used as its fitting curve. The photocarrier lifetime decreases sharply under the early pressure until ~ 2 GPa, and then this rapid decrease gradually slowed down and maintained the slow trend until ~ 8 GPa. We suggest that there might be two main factors to change the photocarrier lifetime: (i) the pressure makes the initial continuous phase transition process of CuS, which leads to the continuous change of the photocarrier lifetime. We have also observed the phenomenon

of different carrier lifetimes in the two phases of one material, such as MoTe_2 .⁵² As the CuS nanoflakes are more sensitive to the pressure at the early time, the rapid change in the initial stage may vary due to this. (ii) This can be attributed to the indirect band structure inherent in the bulk material, which results in a reduced exciton recombination rate due to the necessity of phonon involvement in satisfying the requirement of crystal momentum conservation.⁵³ Shortening the bond length reduces the frequency of phonons moving along the long axis of the unit cell, increases the exciton recombination ratio, and reduces the lifetime. Because the whole experiment is carried out in the linear range between the pump energy density and the peak signal, at this time, the peak value of the differential reflection signal reflecting the carrier life is directly proportional to the carrier density. When the pump power is a fixed value, Figure 2c (green line) shows the monotonic increase trend of carrier density with the increase of pressure. The density of photogenerated carriers rises rapidly in the range of 0–4 GPa and tends to be stable after 4 GPa. The relationship between the differential reflection signal and the density of excited-state carriers in samples is $\Delta R/R_0 = N/N_s$, N is the density of excited-state carriers, while N_s is the density of excited-state carriers when the absorption coefficient decreases to 50% due to photogenerated carriers. It can be obtained that $\Delta R/R_0$ at 4 GPa is 8 times more than that at ambient conditions from Figure 2c. So, compared with ambient conditions, the carrier density under high pressure increases

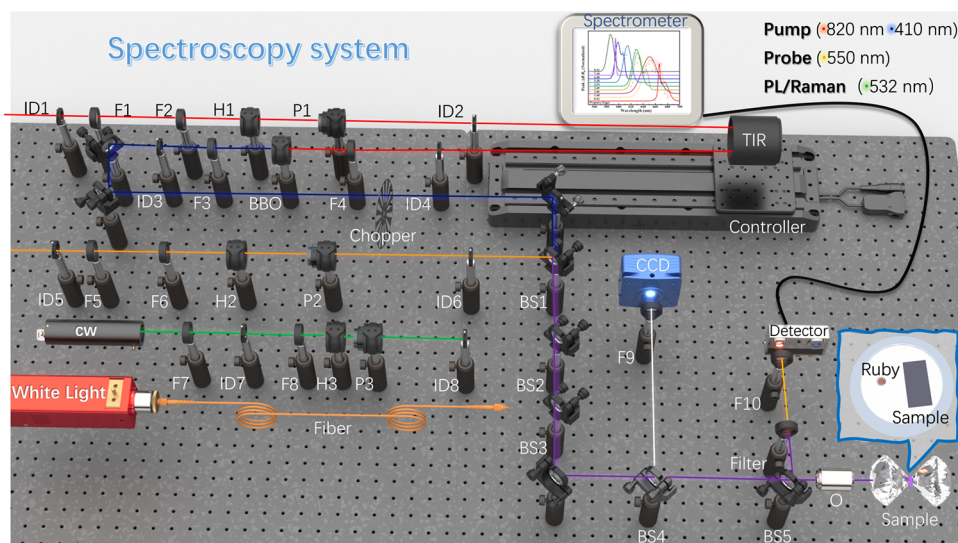


Figure 4. Diagrammatic sketch of the experimental setup for in situ spectroscopy system under pressure. The system is composed of three parts: the collinear microscopy ultrafast pump–probe (transient absorption) system, the cw PL/Raman system, and the white light absorption system. ID: Irises BS: beam splitter; H: half-wavelength plate; P: polarizer; F, focusing lens; BBO: nonlinear crystal; TIR: retroreflector prisms; O, objective lens.

nearly 8 times. With the increase of pressure, the carrier density excited by pump pulse increases, but the overall lifetime shortens to about a quarter of that under ambient conditions, and the carrier dissociation speed increases by nearly 10 times. This result shows that in the process of pressure modulation, the dissociation process of photo-generated carriers accelerates with the increase of pressure, which has a positive impact on the current enhancement of solar cells made of it. It also shows that high-pressure modulation may be one of the effective means to improve the efficiency of solar cells. This discovery also provides theoretical reference for the understanding of CuS in optoelectronic applications under extreme conditions.

CuS owes a hexagonal structure (Figure 3a, left) with space group $P63/mmc$ ($Z = 6$) at ambient conditions⁵⁴ and is not the most stable structure. Instead, the orthorhombic crystal symmetry structure (Figure 3a, right) with space group $Cmcm$ is the thermodynamic ground-state structure,⁵⁵ which will maintain under low temperature (above 55 K).⁵⁶ Previous studies report that the change of CuS material caused by pressurization is similar to that caused by low temperature,⁵⁷ which may lead to CuS moving to a more stable state. The structure of CuS may change from the hexagonal structure to the orthorhombic crystal symmetry, and we call it “translationengleiche,” which is not a sharp but continuous change. For CuS, the tetrahedral site and the trigonal site have different electronic structures with Cu^{2+} centers and Cu^{1+} centers, respectively. According to the first-principle calculation,⁵⁸ the valence band maximum of CuS is mainly contributed by the 3d orbital hybridization of Cu(1) and Cu(2), and the conduction band minimum is mainly donated by the 3s and 3p orbits of S(2). The pressure changes the distance of Cu–S and S–S bonds and the interrelated atomic occupation, then causes the change of electronic structure, and eventually leads to the change of the optical band gap.

In order to further verify our inference, we then carried out Raman spectrum measurement. The hexagonal crystal structure of CuS, by group-theoretical analysis, has the symmetries of the zone-center optical phono modes as follows:

$2A_{1g} + 4B_{2g} + 2E_{1g} + 4E_{2g} + 3A_{2u} + 2B_{1u} + 3E_{1u} + 2E_{2u}$, where eight modes of $2A_{1g} + 2E_{1g} + 4E_{2g}$ are active in the Raman spectra. As shown in Figure 3b, the green and red dashed lines are the Raman spectra of the same CuS nanoflakes under the excitation of 532 and 633 nm continuous laser at ambient conditions. These two modes correspond to $4E_{2g}$, which donate as E_{2g}^4 ($\sim 17 \text{ cm}^{-1}$) and E_{2g}^3 ($\sim 59 \text{ cm}^{-1}$).⁵⁹ We assign ~ 138 and 473 cm^{-1} as A_{1g}^2 and A_{1g}^1 which are thought to be the A_{1g} transverse optic and longitudinal optic (LO) modes, respectively. We suggest that the two modes, ~ 265 and $\sim 947 \text{ cm}^{-1}$, which can only be observed under 532 nm, are E_{2g}^{31} ($\sim 265 \text{ cm}^{-1}$) and the higher-order modes ($\sim 947 \text{ cm}^{-1}$) of LO modes, respectively.

Figure 3c shows the pressure dependence of the vibrational frequencies of CuS. The ~ 17 and $\sim 108 \text{ cm}^{-1}$ mode decrease with pressure. The lowest frequency peak observed at $\sim 17 \text{ cm}^{-1}$ (E_{2g}^4), under ambient conditions, shifts to lower frequencies even beyond the measurement limit with increasing pressure in the spectra at $\sim 4 \text{ GPa}$. This mode has shown the soft mode behavior, which can be attributed to the structure phase transition and implies the possibility of continuous phase transition.⁶⁰ It decreases very rapidly and is consistent with the early pressure-sensitive characteristics of the materials that we mentioned before well. We reported the first observation of the asymmetric mode $\sim 108 \text{ cm}^{-1}$ behavior with the pressure, but it needs further clarification.

On the opposite, as shown in Figure 3d, the modes of A_{1g} increase with pressure. The lower frequency mode at $\sim 138 \text{ cm}^{-1}$ corresponds to the A_{1g}^2 mode related to the motion of Cu(2), which can be assigned to the Cu–S stretching mode, and the higher frequency mode at $\sim 473 \text{ cm}^{-1}$ corresponds to the A_{1g}^1 mode related to the motion of S(2), which can be assigned to the S–S stretching mode. The observed mode strengthening means that the Cu–S pair and S–S pair bond strengths increase with increasing pressure, the same effect as the decrease of the bond length. Undoubtedly, this result proves the inference of the bond length caused by the pressure we mentioned earlier.

In this work, we have effectively tuned the optical band gap structure and photocarrier lifetime in CuS nanoflakes by using pressure engineering via diamond anvil cell (DAC). First, we obtained high-quality CuS nanoflakes on diamond by dry transfer and observed that the direct optical band gap of CuS nanoflakes shows a linear blueshift with the pressure. We propose two possible explanations for this phenomenon: first, the lattice distortion caused by pressure leads to the change of the electronic structure; second, the phase structure changes due to the lattice distortion. Moreover, we find that the photocarrier lifetime decreases significantly with increasing pressure, contributing to the phase transition or the decrease of phonon vibration frequency caused by the pressure. With the increase of pressure, the carrier density excited by the pump pulse increases, but the carrier lifetime shortens to about a quarter of that under ambient conditions, and the carrier dissociation speed increases by nearly 10 times. The result suggests that the dissociation process of photogenerated carriers accelerates under high-pressure modulation, and it may have a positive effect on the current enhancement of solar cells. Raman spectrum reveals the change in Cu–S and S–S bonds and the structural phase transition that may have occurred, consistent with the observed phenomenon. Interestingly, all variations are reversible after decompression, which significantly increases CuS usage scenarios' flexibility. Our work has provided excellent evidence to show that the regulation of pressure on photoelectric properties of CuS improves the competitiveness of CuS and provides theoretical support for subsequent related research. Furthermore, this work suggests the feasibility of using transient absorption spectroscopy (TAS) to explore other materials regulated by pressure for various photonic and optoelectronic applications.

■ EXPERIMENTAL METHODS

Sample Synthesis. CuS microflakes are fabricated by mechanical exfoliation from natural crystals (2D-semiconductor supplies). CuS microflakes are transferred to the diamond directly by the dry-transfer method using polydimethylsiloxane.

Setup for In Situ Measurement. The experimental schematic illustration is shown in Figure 4. We improved the original confocal microscopic TAS and realized the *in situ* measurement and characterization of the absorption, PL, Raman, and transient absorption spectroscopies under high pressure. The sample model in the chamber is shown in the blue box in the lower right corner of Figure 4.

We performed high-pressure measurements in DACs. The DAC made of Mao-Bell alloy with two opposing anvils was used to generate a high pressure. Diamond anvils with 300 μm culets were used for the measurements. This work loaded the sample into the chamber ($D = 150 \mu\text{m}$ hole) in a rhenium gasket preindented to $\sim 40 \mu\text{m}$ in thickness. We chose KBr as the pressure-transmitting medium in our experiments. A ruby ball is loaded to serve as an internal pressure standard, and the pressure is determined by the R1-R2 line shift of the ruby ball.^{61,62} Pressure was measured with an accuracy of 0.1 GPa.

To perform high-pressure absorption measurements, we used a continuous-wave (cw) white light laser with a spot size of $\sim 15 \mu\text{m}$ to excite the sample. For transient absorption, a passive mode-locked Ti-doped sapphire laser was used to generate 100 fs pulses with a central wavelength of 820 nm and a repetition rate of 80 MHz. This pulse is divided into two parts by a beamsplitter. One part pumps an optical parametric oscillator (OPO), which has a signal output in the range of

490–750 nm. The other part of the pulse is sent to a beta barium borate (BBO) crystal to generate its second harmonic at 410 nm. The 410 nm pulse is focused on the sample using an objective lens to a spot size of about 1.7 μm (in fwhm), serving as the pump pulse to excite photocarriers in CuS. The probe pulse is obtained from the output of the OPO with a spot size of 1.8 μm . The reflected probe pulse from the sample is sent to one photodiode of a balanced detector. A portion of the probe pulse is taken before it enters the objective lens and is directly sent to the other photodiode of the balanced detector and used as the reference pulse for the balanced detection.

To perform high-pressure Raman (HORIBA LabRAM HR Evolution RAMAN SPECTROMETER, HORIBA) measurements, a cw 532 and 633 nm laser with a spot size of $\sim 1.7 \mu\text{m}$ was used to excite the sample. The laser power was maintained at approximately 27.8 $\mu\text{J}/\text{cm}^2$ to avoid overheating ring measurements. The spectra for comparison were collected under the same conditions if there were no special instructions. Moreover, all of the measurements were performed at room temperature.

We define *in situ* as all experiments, including pressure calibration, that can be completed without the sample leaving the DAC (its original location) and the experimental light path during the whole investigation. Its advantage is that the influence caused by the possible anisotropy of the model will not be introduced in the testing process to achieve the maximum reliability of the experiment.

■ AUTHOR INFORMATION

Corresponding Authors

Xiaoxian Zhang – Key Laboratory of Luminescence and Optical Information, Ministry of Education, Institute of Optoelectronic Technology, Beijing Jiaotong University, Beijing 100044, China; orcid.org/0000-0002-4215-8274; Email: zhxiaoxian@bjtu.edu.cn

Dawei He – Key Laboratory of Luminescence and Optical Information, Ministry of Education, Institute of Optoelectronic Technology, Beijing Jiaotong University, Beijing 100044, China; Email: dwhe@bjtu.edu.cn

Xiaohui Yu – Beijing National Laboratory for Condensed Matter Physics, Institute of Physics, Chinese Academy of Sciences, Beijing 100190, China; School of Physical Sciences, University of Chinese Academy of Sciences, Beijing 100190, China; Songshan Lake Materials Laboratory, Dongguan 523808, China; orcid.org/0000-0001-8880-2304; Email: yuxh@iphy.ac.cn

Authors

Xiuxian Han – Key Laboratory of Luminescence and Optical Information, Ministry of Education, Institute of Optoelectronic Technology, Beijing Jiaotong University, Beijing 100044, China; orcid.org/0000-0002-2949-8899

Xiaoli Ma – Beijing National Laboratory for Condensed Matter Physics, Institute of Physics, Chinese Academy of Sciences, Beijing 100190, China; orcid.org/0000-0002-8835-4684

Qing Miao – Key Laboratory of Luminescence and Optical Information, Ministry of Education, Institute of Optoelectronic Technology, Beijing Jiaotong University, Beijing 100044, China; orcid.org/0000-0002-5687-3359

Yongsheng Wang – Key Laboratory of Luminescence and Optical Information, Ministry of Education, Institute of

Optoelectronic Technology, Beijing Jiaotong University,
Beijing 100044, China

Complete contact information is available at:

<https://pubs.acs.org/10.1021/acsomega.4c01294>

Author Contributions

X.H. and X.M. contributed equally to this work. All authors have given approval to the final version of manuscript.

Notes

The authors declare no competing financial interest.

ACKNOWLEDGMENTS

We are grateful for the financial support of the National Key R&D Program of China (grant no. 2023YFA1407200), the National Natural Science Foundation of China (grant nos. 62374014 and 11974088), and the Beijing Natural Science Foundation (grant no. 4222073). This work was partially carried out at the high-pressure synergetic measurement station of the Synergetic Extreme Condition User Facility.

REFERENCES

- (1) Gibney, E. The super materials that could trump graphene. *Nature* **2015**, *522*, 274–276.
- (2) Neto, A. H. C.; Novoselov, K. New directions in science and technology: two-dimensional crystals. *Rep. Prog. Phys.* **2011**, *74*, No. 082501.
- (3) Butler, S. Z.; Hollen, S. M.; Cao, L.; Cui, Y.; Gupta, J. A.; Gutiérrez, H. R.; Goldberger, J. E. Progress, Challenges, and Opportunities in Two-Dimensional Materials Beyond Graphene. *ACS Nano* **2013**, *7*, 2898–2926.
- (4) Xi, X.; Wang, Z.; Zhao, W.; Park, J.-H.; Law, K. T.; Berger, H.; Forró, L.; Shan, J.; Mak, K. F. Ising pairing in superconducting NbSe₂ atomic layers. *Nat. Phys.* **2016**, *12*, 139–143.
- (5) Radisavljevic, B.; Kis, A. Mobility engineering and a metal-insulator transition in monolayer MoS(2). *Nature materials* **2013**, *12*, 815–820.
- (6) Yoo, J. J.; Seo, G.; Chua, M. R.; Park, T. G.; Seo, J. J. N. Efficient perovskite solar cells via improved carrier management. *Nature* **2021**, *590*, 587–593.
- (7) Baugher, B. W. H.; Churchill, H. O. H.; Yang, Y.; Jarillo-Herrero, P. Optoelectronic devices based on electrically tunable p–n diodes in a monolayer dichalcogenide. *Nature Nanotechnol.* **2014**, *9*, 262–267.
- (8) Sun, Z.; Martinez, A.; Wang, F. Optical modulators with 2D layered materials. *Nat. Photonics* **2016**, *10*, 227–238.
- (9) Wang, H.; Yu, L.; Lee, Y. H.; Shi, Y.; Hsu, A.; Chin, M. L.; Li, L. J.; Dubey, M.; Kong, J.; Palacios, T. Integrated circuits based on bilayer MoS(2) transistors. *Nano Lett.* **2012**, *12*, 4674–4680.
- (10) Ceballos, F.; Zhao, H. Ultrafast Laser Spectroscopy of Two-Dimensional Materials Beyond Graphene. *Adv. Funct. Mater.* **2017**, *27*, 1604509.
- (11) Wang, R.; Ruzicka, B. A.; Kumar, N.; Bellus, M. Z.; Chiu, H.-Y.; Zhao, H. Ultrafast and spatially resolved studies of charge carriers in atomically thin molybdenum disulfide. *Phys. Rev. B* **2012**, *86*, No. 045406.
- (12) Zhu, C. R.; Zhang, K.; Glazov, M.; Urbaszek, B.; Amand, T.; Ji, Z. W.; Liu, B. L.; Marie, X. Exciton valley dynamics probed by Kerr rotation in WSe₂ monolayers. *Phys. Rev. B* **2014**, *90*, No. 161302.
- (13) Wang, H.; Zhang, C.; Rana, F. Ultrafast dynamics of defect-assisted electron–hole recombination in monolayer MoS₂. *Nano Lett.* **2015**, *15*, 339–345.
- (14) Docherty, C. J.; Parkinson, P.; Joyce, H. J.; Chiu, M. H.; Chen, C.-H.; Lee, M.-Y.; Li, L.-J.; Herz, L. M.; Johnston, M. B. Ultrafast Transient Terahertz Conductivity of Monolayer MoS₂ and WSe₂ Grown by Chemical Vapor Deposition. *ACS Nano* **2014**, *8*, 11147–11153.
- (15) Strait, J. H.; Nene, P.; Rana, F. High intrinsic mobility and ultrafast carrier dynamics in multilayer metal-dichalcogenide MoS₂. *Phys. Rev. B* **2014**, *90*, No. 245402.
- (16) Liu, X.; Yu, H.; Ji, Q.; Gao, Z.; Ge, S.; Qiu, J.; Liu, Z.; Zhang, Y.; Sun, D. An ultrafast terahertz probe of the transient evolution of the charged and neutral phase of photo-excited electron-hole gas in a monolayer semiconductor. *2D Materials* **2016**, *3*, No. 014001.
- (17) Korn, T.; Heydrich, S.; Hirmer, M.; Schmutzler, J.; Schüller, C. Low-temperature photocarrier dynamics in monolayer MoS₂. *Appl. Phys. Lett.* **2011**, *99*, No. 102109.
- (18) Lagarde, D.; Bouet, L.; Marie, X.; Zhu, C. R.; Liu, B. L.; Amand, T.; Tan, P. H.; Urbaszek, B. Carrier and polarization dynamics in monolayer MoS₂. *Phys. Rev. Lett.* **2014**, *112*, No. 047401.
- (19) Wang, G.; Bouet, L.; Lagarde, D.; Vidal, M.; Balocchi, A.; Amand, T.; Marie, X.; Urbaszek, B. Valley dynamics probed through charged and neutral exciton emission in monolayer WSe₂. *Phys. Rev. B* **2014**, *90*, No. 075413.
- (20) Wang, G.; Marie, X.; Bouet, L.; Vidal, M.; Balocchi, A.; Amand, T.; Lagarde, D.; Urbaszek, B. Exciton dynamics in WSe₂ bilayers. *Appl. Phys. Lett.* **2014**, *105*, 182105.
- (21) Pei, S.; Wang, Z.; Xia, J. High pressure studies of 2D materials and heterostructures: A review. *Materials & Design* **2022**, *213*, No. 110363.
- (22) Shirovani, I. I.; Mikami, J.; Adachi, T.; Katayama, Y.; Tsuji, K.; Kawamura, H.; Shimomura, O.; Nakajima, T. Phase transitions and superconductivity of black phosphorus and phosphorus-arsenic alloys at low temperatures and high pressures. *Physical review. B, Condensed matter* **1994**, *50*, 16274–16278.
- (23) Yun, W. S.; Han, S. W.; Hong, S. C.; Kim, I. G.; Lee, J. D. Thickness and strain effects on electronic structures of transition metal dichalcogenides: 2H-MX₂ semiconductors (M = Mo, W; X = S, Se, Te). *Phys. Rev. B* **2012**, *85*, No. 033305.
- (24) Smith, D.; Howie, R. T.; Crowe, I. F.; Simionescu, C. L.; Muryn, C.; Vishnyakov, V.; Proctor, J. E. Hydrogenation of graphene by reaction at high pressure and high temperature. *ACS Nano* **2015**, *9*, 8279–8283.
- (25) Huang, G.-Q.; Xing, Z.-W. Superconductivity of bilayer phosphorene under interlayer compression. *Chinese Physics B* **2016**, *25*, No. 027402.
- (26) Liu, F.; Zhou, J.; Zhu, C.; Liu, Z. Electric Field Effect in Two-Dimensional Transition Metal Dichalcogenides. *Adv. Funct. Mater.* **2017**, *27*, 27.
- (27) Huang, B.; Clark, G.; Navarro-Moratalla, E.; Klein, D. R.; Cheng, R.; Seyler, K. L.; Zhong, D.; Schmidgall, E.; McGuire, M. A.; Cobden, D. H.; Yao, W.; Xiao, D.; Jarillo-Herrero, P.; Xu, X. Layer-dependent ferromagnetism in a van der Waals crystal down to the monolayer limit. *Nature* **2017**, *546*, 270–273.
- (28) Segura, A.; Cuscó, R.; Taniguchi, T.; Watanabe, K.; Cassabois, G.; Gil, B.; Artús, L. High-Pressure Softening of the Out-of-Plane A_{2u} (Transverse-Optic) Mode of Hexagonal Boron Nitride Induced by Dynamical Buckling. *J. Phys. Chem. C* **2019**, *123*, 17491–17497.
- (29) Liu, Y.; Zhang, S.; He, J.; Wang, Z. M.; Liu, Z. Recent Progress in the Fabrication, Properties, and Devices of Heterostructures Based on 2D Materials. *Nano-micro letters* **2019**, *11*, 1–24.
- (30) Wan, X.; Li, H.; Chen, K.; Xu, J. Towards Scalable Fabrications and Applications of 2D Layered Material-based Vertical and Lateral Heterostructures. *Chemical Research in Chinese Universities* **2020**, *36*, 525–550.
- (31) Fu, L.; Wan, Y.; Tang, N.; Ding, Y. M.; Gao, J.; Yu, J.; Shen, B. K–Λ crossover transition in the conduction band of monolayer MoS₂ under hydrostatic pressure. *Sci. Adv.* **2017**, *3* (11), No. e1700162.
- (32) Zhao, Z.; Zhang, H.; Yuan, H.; Wang, S.; Lin, Y.; Zeng, Q.; Xu, G.; Liu, Z.; Solanki, G. K.; Patel, K. D.; Cui, Y.; Hwang, H. Y.; Mao, W. L. Pressure induced metallization with absence of structural transition in layered molybdenum diselenide. *Nat. Commun.* **2015**, *6*, 7312.
- (33) Nayak, A. P.; Yuan, Z.; Cao, B.; Liu, J.; Wu, J.; Moran, S. T.; Li, T.; Akinwande, D.; Jin, C.; Lin, J. F. Pressure-Modulated

- Conductivity, Carrier Density, and Mobility of Multilayered Tungsten Disulfide. *ACS Nano* **2015**, *9*, 9117–9123.
- (34) Nayak, A. P.; Bhattacharyya, S.; Zhu, J.; Liu, J.; Wu, X.; Pandey, T.; Jin, C.; Singh, A. K.; Akinwande, D.; Lin, J. F. Pressure-induced semiconducting to metallic transition in multilayered molybdenum disulfide. *Nat. Commun.* **2014**, *5*, 3731.
- (35) Guo, S.; Bu, K.; Li, J.; Hu, Q. Enhanced Photocurrent of All-Inorganic Two-Dimensional Perovskite $\text{Cs}_2\text{PbI}_2\text{Cl}_2$ via Pressure-Regulated Excitonic Features. *J. Am. Chem. Soc.* **2021**, *143*, 2545–2551.
- (36) Xia, J.; Yan, J.; Wang, Z.; He, Y.; Gong, Y.; Chen, W.; Sum, T. C.; Liu, Z.; Ajayan, P. M.; Shen, Z. Strong coupling and pressure engineering in WSe_2 - MoSe_2 heterobilayers. *Nat. Phys.* **2021**, *17*, 92–98.
- (37) Ma, X.; Fu, S.; Ding, J.; Liu, M.; Bian, A.; Hong, F.; Sun, J.; Zhang, X.; Yu, X.; He, D. Robust Interlayer Exciton in $\text{WS}_2/\text{MoSe}_2$ van der Waals Heterostructure under High Pressure. *Nano Lett.* **2021**, *21*, 8035–8042.
- (38) Guo, S.; Zhao, Y.; Bu, K.; Fu, Y.; Luo, H.; Chen, M.; Hautzinger, M. P.; Wang, Y.; Jin, S.; Yang, W. Pressure-Suppressed Carrier Trapping Leads to Enhanced Emission in Two-Dimensional Perovskite $(\text{HA})_2(\text{GA})\text{Pb}_2\text{I}_7$. *Angew. Chem.* **2020**, *132*, 17686–17692.
- (39) Li, M.; Liu, T.; Wang, Y.; Yang, W.; Matter, X. L. J.; Extremes, R.; a. Pressure responses of halide perovskites with various compositions, dimensionalities, and morphologies. *Matter Radiat. Extremes* **2020**, *5*, No. 018201.
- (40) Lei, H.; Fang, G.; Cheng, F.; Ke, W.; Qin, P. Enhanced efficiency in organic solar cells via in situ fabricated p-type copper sulfide as the hole transporting layer. *Sol. Energy Mater. Sol. Cells* **2014**, *128*, 77–84.
- (41) Bhargav, R.; Patra, A.; Dhawan, S. K.; Gairola, S. P. J. S. E. Solution processed hole transport layer towards efficient and cost effective organic solar cells. *Sol. Energy* **2018**, *165*, 131–135.
- (42) Zeng, H.; Liu, G. B.; Dai, J.; Yan, Y.; Zhu, B.; He, R.; Xie, L.; Xu, S.; Chen, X.; Yao, W.; Cui, X. Optical signature of symmetry variations and spin-valley coupling in atomically thin tungsten dichalcogenides. *Sci. Rep.* **2013**, *3*, 1608.
- (43) Choi, H.; Lee, J. P.; Ko, S. J.; Jung, J. W.; Park, H.; Yoo, S.; Park, O.; Jeong, J. R.; Park, S.; Kim, J. Y. Multipositional Silica-Coated Silver Nanoparticles for High-Performance Polymer Solar Cells. *Nano Lett.* **2013**, *13*, 2204.
- (44) Yin, X.; Ye, Z.; Chenet, D. A.; Ye, Y.; O'Brien, K.; Hone, J. C.; Zhang, X. J. E. Edge Nonlinear Optics on a MoS_2 Atomic Monolayer. *Science* **2014**, *344*, 488–490.
- (45) Hu, C.; Wang, X.; Song, B. High-performance position-sensitive detector based on the lateral photoelectrical effect of two-dimensional materials. *Light: Sci. Appl.* **2020**, *9*, 88.
- (46) Mak, K. F.; Sfeir, M. Y.; Wu, Y.; Lui, C. H.; Misewich, J. A.; Heinz, T. F. Measurement Of The Optical Conductivity Of Graphene. *Phys. Rev. Lett.* **2008**, *101*, No. 196405.
- (47) Ma, X.; Fu, S.; Ding, J.; Liu, M.; Bian, A.; Hong, F.; Sun, J. T.; Zhang, X.; Yu, X.; He, D. Pressure-enhanced interlayer exciton in $\text{WS}_2/\text{MoSe}_2$ van der Waals heterostructure. *Nano Lett.* **2021**, *21*, 8035–8042.
- (48) Miao, Q.; He, D.; Han, X.; Hao, S.; Zhao, H. Spatiotemporally Resolved Optical Measurements on Photocarrier Dynamics in Copper Monosulfide. *J. Phys. Chem. C* **2020**, *124*, 14459–14464.
- (49) Ceballos, F.; Cui, Q.; Bellus, M. Z.; Zhao, H. Exciton formation in monolayer transition metal dichalcogenides. *Nanoscale* **2016**, *8* (22), 11681–11688.
- (50) Ludwig, J.; An, L.; Pattengale, B.; Kong, Q.; Zhang, X. Ultrafast Hole Trapping and Relaxation Dynamics in p-Type CuS Nanodisks. *J. Phys. Chem. Lett.* **2015**, *6*, 2671–2675.
- (51) Bykov, A. Y.; Shukla, A.; van Schilfgaarde, M.; Green, M. A.; Zayats, A. V. Ultrafast Carrier and Lattice Dynamics in Plasmonic Nanocrystalline Copper Sulfide Films. *Laser & Photonics Reviews* **2021**, *15*, No. 2000346.
- (52) Han, X.; Liang, X.; He, D.; Jiao, L.; Wang, Y.; Zhao, H. Photocarrier Dynamics in MoTe_2 Nanofilms with $2H$ and Distorted $1T$ Lattice Structures. *ACS Appl. Mater. Interfaces* **2021**, *13*, 44703–44710.
- (53) He, J.; He, D.; Wang, Y.; Cui, Q.; Hui, Z. Spatiotemporal dynamics of excitons in monolayer and bulk WS_2 . *Nanoscale* **2015**, *7*, 9526–9531.
- (54) Morales-García, A.; Soares, A. L., Jr; Dos Santos, E. C.; de Abreu, H. A.; Duarte, H. A. First-Principles Calculations and Electron Density Topological Analysis of Covellite (CuS). *J. Phys. Chem. A* **2014**, *118*, 5823–5831.
- (55) Liang, W.; Whangbo, M. H. Conductivity anisotropy and structural phase transition in Covellite CuS . *Solid state communications* **1993**, *85*, 405–408.
- (56) Fjellvåg, H.; Grønvold, F.; Stølen, S.; Andresen, A. F.; Müller-Käfer, R.; Simon, A. Low-temperature structural distortion in CuS . *Z. Kristallogr.* **1988**, *184*, 111–121.
- (57) Peiris, S. M.; Sweeney, J. S.; Campbell, A. J.; Heinz, D. L. Pressure-induced amorphization of covellite, CuS . *J. Chem. Phys.* **1996**, *104*, 11–16.
- (58) Arora, S.; Kabra, K.; Joshi, K. B.; Sharma, B. K.; Sharma, G. J. P. B. C. M. Structural, elastic, thermodynamic and electronic properties of Covellite, CuS . *Physica B: Condensed Matter* **2020**, *582*, No. 311142.
- (59) Xin, Z.; Tan, Q. H.; Wu, J. B.; Wei, S.; Tan, P. H. Review on the Raman spectroscopy of different types of layered materials. *Nanoscale* **2016**, *8*, 6435–6450.
- (60) Scott, J. Soft-mode spectroscopy: Experimental studies of structural phase transitions. *Rev. Mod. Phys.* **1974**, *46*, 83.
- (61) Liang, A.; Turnbull, R.; Bandiello, E.; Yousef, I.; Errandonea, D. High-pressure spectroscopy study of $\text{Zn}(\text{IO}_3)_2$ using far-infrared synchrotron radiation. *Crystals* **2020**, *11* (1), 34.
- (62) Mao, H. K.; Bell, P. M.; Shaner, J. W.; Steinberg, D. J. Specific volume measurements of Cu, Mo, Pd, and Ag and calibration of the ruby R1 fluorescence pressure gauge from 0.06 to 1 Mbar. *J. Appl. Phys.* **1978**, *49* (6), 3276–3283.